

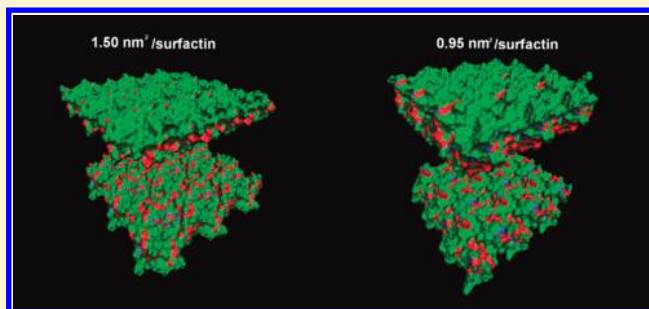
Molecular Dynamics Study of Surfactin Monolayer at the Air/Water Interface

Hong-Ze Gang, Jin-Feng Liu, and Bo-Zhong Mu*

State Key Laboratory of Bioreactor Engineering and Institute of Applied Chemistry, East China University of Science and Technology, Shanghai, People's Republic of China 200237

S Supporting Information

ABSTRACT: The surface parameter of protonated surfactin molecules and the structural properties of the protonated surfactin monolayer adsorbed at the air/water interface have been studied by molecular dynamics simulation. The simulation was performed at 293 K and the interfacial concentration of surfactin was set in a range of 0.70–2.20 nm² molecule^{−1}. The results show that the interfacial concentration greatly affects the molecular orientation of surfactin, the structure of the peptide ring backbone and the spatial arrangement of the surfactin monolayer. The peptide ring backbone of the surfactin molecule exhibits a structural flexibility, and a more packed structure is adopted at higher interfacial concentration. The hydrophobic contacts between surfactin molecules and the stability of the secondary structures, β -turn structure in Leu2 \rightarrow Asp5 and the β -sheet domains, are enhanced when the surfactin molecules are in a very packed situation.



1. INTRODUCTION

Surfactin, a general term for a class of cyclic lipopeptides, is considered as one of the most powerful biosurfactants for its prominent interfacial activity. Surfactin consists of a heptapeptide linked to a β -hydroxy fatty acid and closed via a lactone bond, and the length of the fatty acid chain varies from C12 to C17.^{1–3} Earlier studies showed that surfactin could lower the surface tension of aqueous solution from 72 to \sim 30 mN m^{−1} at a concentration of the order 10^{−5} M.^{4,5} Surfactin also had been demonstrated to exhibit antiviral,⁶ antifungal,⁷ and hemolytic properties.⁸ These remarkable physicochemical and biological properties hold promise for the potential application of surfactin in microbial enhanced oil recovery,⁹ bioremediation of the environmental pollutant,¹⁰ and pharmacological research.⁶

The investigation of surfactin molecules at the air/water interface is of crucial role in understanding the surfactin interfacial properties. Maget-Dana and Ptak¹¹ reported the interfacial behavior of surfactin molecules at the air/water interface and studied the influence of pH, temperature and the addition of electrolytes in the subphase on the shape of the compression isotherm curves of surfactin monolayer, and several orientations of surfactin molecules were presumed. Ishigami et al.⁴ suggested that surfactin molecules organized at the air/water interface in a β -sheet secondary structure. In the molecular modeling of Gallet et al.,¹² a design of surfactin conformation was illustrated to correspond to the experimental behavior of surfactin in weak compression, in which the peptide ring was positioned in the plane of the interface with the two acidic amino acid residues protruding in the aqueous phase and the aliphatic chain folded

back to interact mainly with the Leu2 and Val4 side chains. Nicolas¹³ demonstrated in his simulation that the peptidic backbone of surfactin exhibited a large flexibility at the hexane/water interface and the structural fluctuations depended strongly on the interfacial concentration. Song et al.¹⁴ investigated the surfactin monolayer by a Langmuir–Blodgett film balance combined with atomic force microscopy, and concluded that surfactin organized in distinct patterns with different physical states. Recently, surfactin structure at the air/water interface had been studied by neutron reflectometry,^{15,16} and the results showed that surfactin had a hydrophobic ball-like structure, and the hydrophilicity of surfactin was affected by its charge and the addition of cations. However, the insight information of the surface parameter of surfactin at the air/water interface and the structural properties of surfactin monolayer at a molecular level is still limited.

Molecular dynamics simulation provides an opportunity to study the details of the monolayer interactions at a molecular level which are not accessible by experimental techniques. The focus of the present simulation is the surface parameter of protonated surfactin molecules and the structure of the protonated surfactin monolayer adsorbed at the air/water interface. The influence of the interfacial concentration on the molecular orientation, the structure, and the spatial arrangement of surfactin monolayer were studied. The structure of the surfactin

Received: July 5, 2011

Revised: August 31, 2011

Published: September 29, 2011

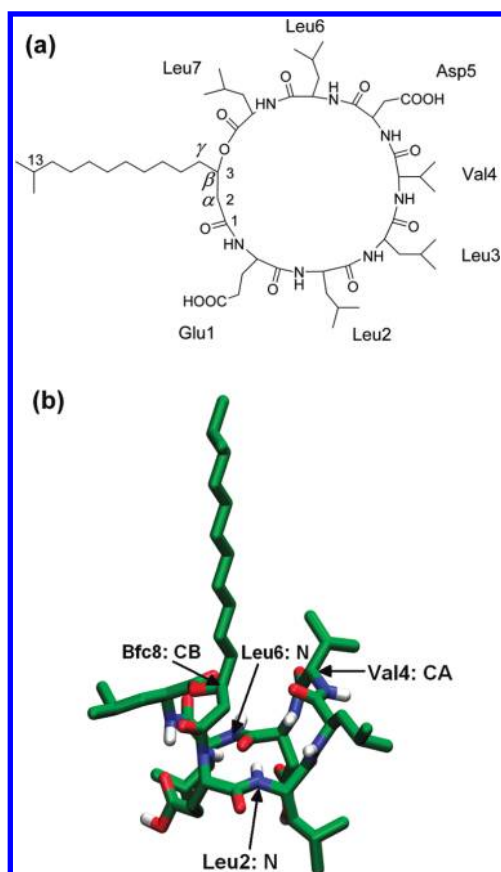


Figure 1. (a) Chemical composition and (b) secondary structure of *iso*-C15 surfactin. The atom coloring scheme is C, green; N, blue; O, red; and H, white. For visual clarity, all of the nonpolar hydrogen atoms are not displayed. Conformation graphs in this paper are all produced with VMD software.¹⁹

monolayer was investigated by the monolayer width and the surface pressure–area isotherm, and the limiting molecular area of surfactin molecule and the compressibility constant of the monolayer were consequently estimated.

2. SIMULATION METHODS

Surfactin used in the present simulation is the *iso*-C15 surfactin (15 denotes the carbon number in the β -hydroxy fatty acid moiety), and its chemical structure is given in Figure 1a. The peptide ring backbone of surfactin molecule adopts a “horse-saddle” conformation proposed by Bonmatin,¹⁷ and its secondary structure can be seen in Figure 1b. The peptide ring moiety was considered as the surfactin headgroup, and the remainder aliphatic chain that from the γ carbon atom was taken as surfactin tail. The limiting molecular area, A_0 , and the transition area, A_t , of protonated surfactin molecule at the air/water interface reported in previous literatures were 1.54–2.20 nm² and 1.03–1.44 nm², respectively.^{11,12,14,18} Therefore, the molecular area of surfactin was set in a range of 0.70–2.20 nm² in our simulation, and we believed that the present simulation can represent the change of expanded situation to the condensed situation of the protonated surfactin monolayer at the air/water interface.

A series of simulations were performed for different interfacial concentrations of surfactin molecules at the air/water interface. The setup steps of all the simulations were the same as follows.

Table 1. Computational Details of the Different Simulations

area per surfactin molecule (nm ²)	$L_x \times L_y$ (nm \times nm)	surfactin number	total number of atoms
0.70	3.347 \times 3.347	2 \times 16	10 928
0.95	2.924 \times 2.924	2 \times 9	7296
1.20	3.286 \times 3.286	2 \times 9	8361
1.35	3.486 \times 3.486	2 \times 9	8985
1.50	3.674 \times 3.674	2 \times 9	9744
1.80	2.683 \times 2.683	2 \times 4	4901
2.20	2.966 \times 2.966	2 \times 4	5762

First, a box was filled with simple point charge water molecules²⁰ and equilibrated at 293 K for 300 ps, and then the water box was centered in a cube which has the same L_x and L_y dimensions and a size of 15 nm in the z direction. Second, two layers of surfactin molecules were arranged and placed on the two opposite air/water interfaces with their acidic amino acids residues, Glu1 and Asp5, and most of their peptide ring backbones solvated. After that, energy minimization was performed using steepest descent. Third, a period of 8 ns MD simulation was applied to the system by a time step of 2 fs, and the equilibration of the simulation was checked by monitoring the potential energy as well as the root-mean-square deviation of the peptide ring backbones. The thick of the water slab was roughly 5 nm and the interfacial concentration was controlled by the area of xy plane and the number of surfactin molecule in the two layers. The computational details of each MD simulation were given in Table 1.

The Gromacs 3.3.1 package^{21,22} and the OPLS force field²³ were used to run all the MD simulations in the NVT ensemble. Berendsen thermostat²⁴ was applied to maintain the system temperature at 293 K, and the coupling time constant was 0.1 ps. The cutoff radius of both van der Waals interactions and the real part of electrostatic interactions was 1.0 nm. Electrostatic forces were calculated using particle mesh Ewald method²⁵ with precision 10^{-4} . All bond lengths were constrained using SHAKE algorithm²⁶ with tolerance 10^{-4} , and the periodic condition was applied in all the three directions. MD trajectories were collected every 1.0 ps and the last 6 ns run was used for analysis.

3. RESULTS

3.1. Density Distributions. The atom density distributions of surfactin, surfactin headgroups, hydrophobic tails and water are separately estimated and shown in Figure 2. As can be clearly seen in the figure, the density distribution of surfactin exhibits a normal distribution at the air/water interface at low surface coverage and the distribution expands with the increase of the interfacial concentration, and significant deviations from the normal distribution are observed when the interfacial concentration exceeds a value of 0.95 nm² molecule⁻¹. Similar varieties in profile pattern are also found for the atom density distributions of surfactin headgroups and hydrophobic tails. Moreover, the extremely wide and nonuniform density distribution of surfactin at the highest interfacial concentration in our simulation, 0.70 nm² molecule⁻¹, indicates a disorder monolayer that over compressed at the air/water interface.

The atom density distributions of surfactin, surfactin headgroups and hydrophobic tails at each air/water interface are separately fitted by Gaussian formula²⁷ to estimate their distribution widths and to

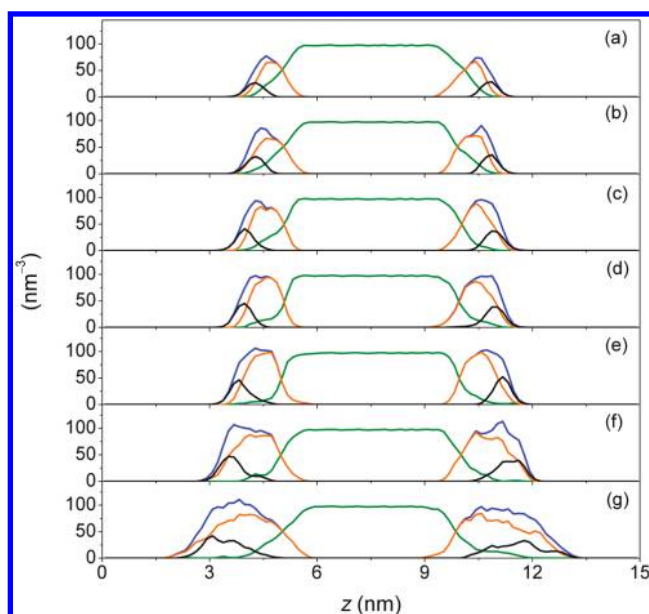


Figure 2. Atom density distributions of surfactin (blue), surfactin headgroups (orange), hydrophobic tails (black) and water (green) at (a) 2.20, (b) 1.80, (c) 1.50, (d) 1.35, (e) 1.20, (f) 0.95, and (g) 0.70 nm² molecule⁻¹.

Table 2. Distribution Widths of Surfactin, σ_{SF} , Headgroups, σ_{Head} , Hydrophobic Tails, σ_{Tail} , and the Separation Distance between the Centers of the Distributions of Headgroup and Hydrophobic Tail, δ_{H-T} ^a

area per surfactin molecule (nm ²)	σ_{SF} (nm)	σ_{Head} (nm)	σ_{Tail} (nm)	δ_{H-T} (nm)
0.95	1.83 ± 0.01	1.69 ± 0.04	0.97 ± 0.15	0.69 ± 0.03
1.20	1.43 ± 0.04	1.19 ± 0.02	0.70 ± 0.07	0.65 ± 0.01
1.35	1.34 ± 0.01	1.16 ± 0.09	0.70 ± 0.05	0.57 ± 0.09
1.50	1.28 ± 0.06	1.12 ± 0.01	0.70 ± 0.04	0.54 ± 0.09
1.80	1.22 ± 0.01	1.12 ± 0.08	0.66 ± 0.04	0.48 ± 0.06
2.20	1.14 ± 0.05	0.99 ± 0.04	0.67 ± 0.04	0.49 ± 0.03

^a The errors are obtained from the average value of the two air/water interfaces.

locate the centers of distributions in z direction. Table 2 lists the distribution widths of surfactin, surfactin headgroups and hydrophobic tails, as well as the separation distances between the centers of distributions of headgroups and hydrophobic tails. It appears that the distribution widths of the surfactin molecules and the surfactin headgroups, σ_{SF} and σ_{Head} , smoothly increase with the interfacial concentration, however, the distribution width of the hydrophobic tails, σ_{Tail} , nearly keeps a constant value when the interfacial concentration varies in a range of 1.20–2.20 nm² molecule⁻¹. When the molecular area decreases from 1.20 nm² to 0.95 nm², about 28%, 42%, and 39% increment are estimated for σ_{SF} , σ_{Head} , and σ_{Tail} respectively. These significant expansions in distribution widths are mainly assigned to the more compact situation and the reorientation of surfactin molecules at the air/water interface. In addition, the separation distance between the centers of the distributions of the headgroups and the hydrophobic tail, δ_{H-T} , increases gently and achieves a maximum separation of 0.69 nm, implying a close

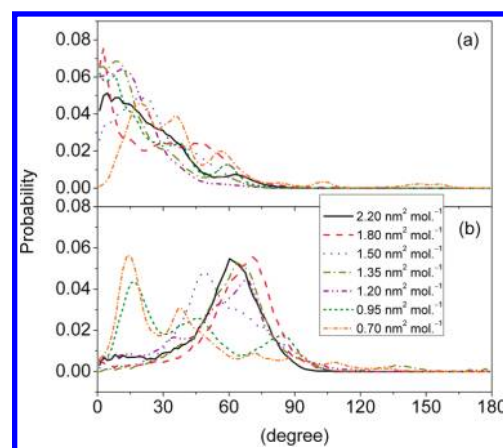


Figure 3. Normalized probability distribution of (a) α_H , the angle of V_H respect to the normal to the interface and (b) α_T , the angle of V_T respect to the normal to the interface. V_H is defined as the vector product of the CC vector and NN vector, and V_T is defined as the vector connecting the carbon atom C₃ and the carbon atom C₁₃.

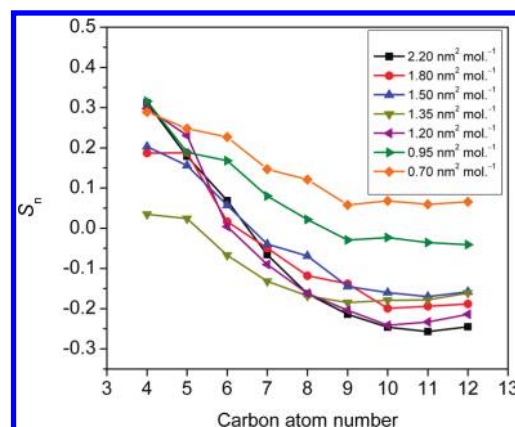


Figure 4. Order parameter, S_n , of $C_{n-1}C_{n+1}$ vector in surfactin tail, n is the carbon number noted in the primary structure of surfactin shown in Figure 1a.

relationship between the headgroup and the hydrophobic tail in spatial distribution, which can be attribute to the hydrophobic contact between the aliphatic tail and the hydrophobic side chains in the headgroup.

3.2. Surfactin Orientation. The orientation of surfactin molecules at the air/water interface are investigated by the orientation of the characteristic vectors defined in the headgroup and the hydrophobic tail. In the surfactin headgroup, the vector product of the CC vector and the NN vector that pointed from the hydrophilic side to the hydrophobic side of the “horse-saddle” conformation of the peptide ring backbone, V_H , is taken as the characteristic vector. As shown in Figure 1b, the CC vector is defined as the vector connecting the β carbon atom of the fatty acid residue (Bfc: CB) and the α carbon atom in Val4 residue (Val4: CA), the vector that connects the nitrogen atom of Leu2 residue (Leu2: N) and the nitrogen atom of Leu6 residue (Leu6: N) is defined as the NN vector. In the hydrophobic tail, the vector connecting the carbon atom C₃ and the carbon atom C₁₃, V_T , is monitored. Figure 3 shows the normalized angular distribution of α_H and α_T , the angles of V_H and V_T respect to the normal to the interface (from bulk water to vacuum). As can be seen in the figure,

stable angular distributions are observed both for α_H and α_T at lower interfacial concentration. The main contributions in a range of 0° – 40° of α_H show that most of the peptide ring backbones slightly tilt at the air/water interface in a supine position, and the angular distribution of α_T exhibits a main peak centered on 45° – 85° suggesting that the hydrophobic tails intend to approach the air/water interface. The angular distribution of α_H drifts toward higher angle value at an interfacial concentration of $0.70 \text{ nm}^2 \text{ molecule}^{-1}$ and the angular distribution of α_T drifts toward lower angle value when the interfacial concentration exceeds $0.95 \text{ nm}^2 \text{ molecule}^{-1}$. It implies that surfactin molecules reorientated in a more packed situation, and the final orientation is that both the peptide ring backbones and the hydrophobic tails adopt a more tilted orientation at the air/water interface. Minor contributions $>90^\circ$ of the angular distribution of α_H at an interfacial concentration of $0.70 \text{ nm}^2 \text{ molecule}^{-1}$ corresponds to the presence of the tumbled-over molecules, which are mainly the result of the disorder distribution of surfactin molecules at the air/water interface. Further estimation indicates that the hydrophobic side chains in the surfactin head-group adopt a more tilted orientation at higher interfacial concentration, and these tilted orientations benefit the spatial arrangement of the surfactin headgroups in organizing a more packed monolayer at the air/water interface.

The order parameter, $S_n = \langle 3 \cos^2(\alpha_n) - 1 \rangle / 2$,²⁸ of the carbon atoms in the hydrophobic tails is computed to get the detail information of the orientation of surfactin tails, where α_n is the angle between $C_{n-1}C_{n+1}$ vector and the normal to the interface. As can be seen in Figure 4, the order parameter descends close to zero at a molecular area of 0.95 nm^2 and to a set of negative values at lower interfacial concentration as a function of the increase of the carbon atom number. The terminal parts of the hydrophobic tails behavior an isotropic orientation around the normal to the interface at an interfacial concentration of $0.95 \text{ nm}^2 \text{ molecule}^{-1}$, and the terminal parts intend to parallel the air/water interface at the interfacial concentration lower than $0.95 \text{ nm}^2 \text{ molecule}^{-1}$. The positive value of the order parameter obtained at the terminal part of the hydrophobic tails at $0.70 \text{ nm}^2 \text{ molecule}^{-1}$ implies that the hydrophobic tails intend to vertically orientate at the air/water interface.

Hydrophobic contact is the most reasonable illustration for the close relationship between the headgroup and the hydrophobic tail in spatial distribution as well as the tilted orientation of the hydrophobic tails at a higher interfacial concentration as concluded above. Although the surfactin molecule consists of only eight residues (seven amino acid residues and one fatty acid residue), a method used for monitoring the minimum distances between the residues within a protein molecule²⁹ is employed to estimate the hydrophobic contact between the residues within a surfactin molecule or belong to different surfactin molecules. Figure S1 of the Supporting Information, SI, displays the averaged matrix of the smallest distance between the residues, and a cutoff distance of 0.35 nm is used to determine whether a hydrophobic contact occurs. It is clearly shown in the figure that the hydrophobic tails (the residue number is an integer multiple of 8) are favorite to interact with the amino acid residues within the same molecule, where the Leu3 and the Val4 are the residues that the hydrophobic tails preferentially contact with. Moreover, surfactin tails also exhibit intermolecular hydrophobic contact with both the amino acid residue and the hydrophobic tail. Intramolecular and intermolecular hydrophobic contacts between the amino acid residues are also observed, but the frequency of these hydrophobic contacts is lower than that between the hydrophobic tails. Intermolecular hydrophobic

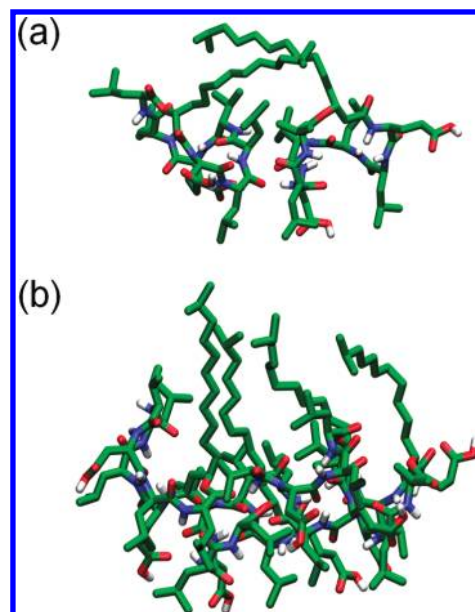


Figure 5. Side views of surfactin molecules at (a) 2.20 and (b) $0.95 \text{ nm}^2 \text{ molecule}^{-1}$. The atom coloring scheme is C, green; N, blue; O, red; and H, white. For visual clarity, all of the nonpolar hydrogen atoms are not displayed.

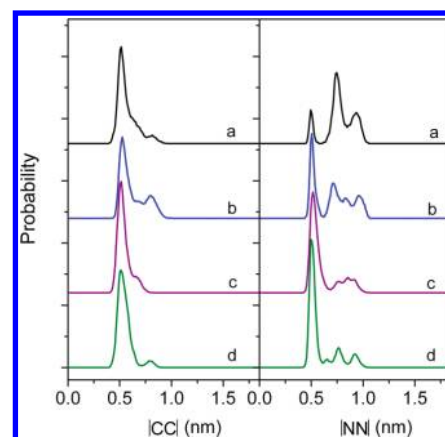


Figure 6. Normalized probability distribution of CC and NN magnitudes, a–d corresponds to the interfacial concentration of 2.20 , 1.50 , 1.20 , and $0.95 \text{ nm}^2 \text{ molecule}^{-1}$ respectively.

contacts are enhanced with the increase of the interfacial concentration, resulting in a more packed spatial distribution of surfactin molecules at the air/water interface.

Figure 5 depicts two representative side views of surfactin molecules at the air/water interface. At a lower interfacial concentration of $2.20 \text{ nm}^2 \text{ molecule}^{-1}$ two surfactin molecules gather together by their hydrophobic tails and the tails nearly parallel the interface. It should be noted here that both the hydrophobic tails locate in the upper region of the aggregate that far away from bulk water. While at a higher interfacial concentration of $0.95 \text{ nm}^2 \text{ molecule}^{-1}$, as shown in Figure 5b, the surfactin molecule is able to closely contact with the surrounding molecules, and the hydrophobic tails interact with each other to form a bundle which more vertically tilts at the air/water interface.

3.3. Surfactin Structure and Spatial Arrangement. The orientation distribution of the peptide ring backbones showed

Table 3. Occupancy of the Intramolecular Hydrogen Bonds, HB_{SSI} , the Intermolecular Hydrogen Bonds, HB_{SSO} , and the Hydrogen Bonds Formed between Surfactin Molecule and Water, HB_{SW}

area per surfactin molecule (nm^2)	hydrogen bonds occupancy (%)		
	HB_{SSI}	HB_{SSO}	HB_{SW}
0.70	24.8	13.3	30.9
0.95	25.7	14.4	31.5
1.20	24.8	11.2	40.3
1.35	22.4	6.6	48.5
1.50	18.7	5.4	52.7
1.80	14.9	8.4	56.3
2.20	15.4	5.6	57.5

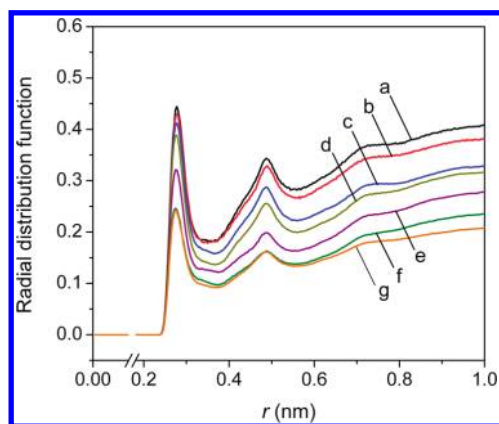


Figure 7. Radial distribution functions of the heavy atoms (oxygen and nitrogen) with water oxygen atoms, normalized by the bulk density of water phase, a–g corresponds to the interfacial concentration of 2.20, 1.80, 1.50, 1.35, 1.20, 0.95, and $0.70 \text{ nm}^2 \text{ molecule}^{-1}$, respectively.

that the “horse-saddle” conformation of the peptide ring backbones persisted for a supine position and slightly tilted at the interface in a wide interfacial concentration range of $0.95\text{--}2.20 \text{ nm}^2 \text{ molecule}^{-1}$, thus we suggest that the peptide ring backbones exhibit a structural flexibility at the air/water interface. For example, the “horse-saddle” conformation of the peptide ring backbone presents a more compact structure at higher interfacial concentration to keep a supine orientation at the air/water interface.

Here the normalized length distributions of the CC and NN vectors are evaluated to detect the spans of the hydrophobic and the hydrophilic side of the “horse-saddle” conformation of the peptide ring backbones. As can be seen in Figure 6, the length of CC vectors is $\sim 0.52 \text{ nm}$, and at higher interfacial concentration the NN magnitude is $\sim 0.5 \text{ nm}$. The length of NN vectors shows a broad distribution at lower interfacial concentration, and main contribution $>0.75 \text{ nm}$ is measured. It is distinct that the peptide ring backbones expand at lower interfacial concentration especially in the hydrophilic span, and a more compact geometry structure is adopted at higher interfacial concentration. In addition, the root-mean-square deviations of the peptide ring backbones (N, C_ω , C atoms in amino acid residues and C, C_ω , C_β , O atoms in the fatty acid residue) and the Ramachandran angles are monitored, and the results also display that the higher interfacial concentration is the smaller variations in structure and the more concentrative distribution of Ramachandran angles become.

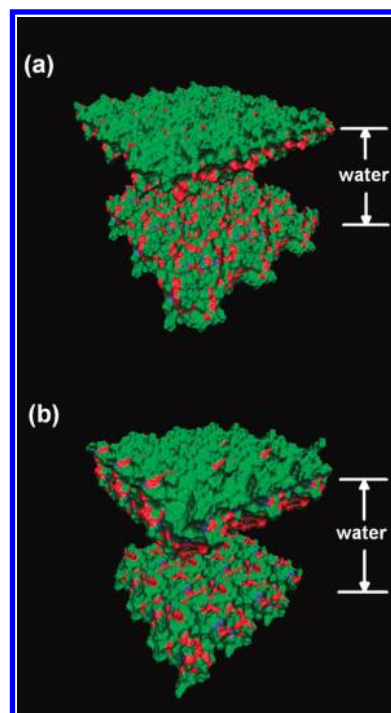


Figure 8. Surfaces of the hydrophobic and hydrophilic sides of the surfactin monolayer at (a) 1.50 and (b) $0.95 \text{ nm}^2 \text{ molecule}^{-1}$. The coloring scheme is as follows: carbonyl group in the peptide bonds and the carboxyl groups in Glu1 and Asp5, red; amino group in the peptide bonds, blue; nonpolar carbon and hydrogen atoms, green.

Surfactin molecules exhibit a more compact structure at a higher interfacial concentration, and thus the formation of the intramolecular hydrogen bonds (HB_{SSI}) and intermolecular hydrogen bonds (HB_{SSO}) are also affected. Table 3 gives the hydrogen bond occupancy of HB_{SSI} and HB_{SSO} , and both of them behavior an ascending trend with the increase of the interfacial concentration. The hydrogen donors and acceptors in surfactin molecules form preferentially intramolecular hydrogen bonds rather than intermolecular hydrogen bonds. Intramolecular hydrogen bonds that represent the β -turn secondary structure in $\text{Leu2} \rightarrow \text{Asp5}$ segment are detected and its occurrence probability almost-positively correlates with the interfacial concentration, and a maximum proportion of 17.8% is achieved at an interfacial concentration of $0.95 \text{ nm}^2 \text{ molecule}^{-1}$. The occupancy of HB_{SSI} and HB_{SSO} exhibits a considerable increase throughout and these hydrogen bonds are carefully monitored to locate a β -sheet conformation. The hydrogen bonds presented the β -sheet conformation are observed within and between the peptide ring backbones, and the β -sheet domains behavior more stable at higher interfacial concentration. However, the presence of β -sheet domain is in small quantity, especially the β -sheet conformation formed between surfactin molecules. Though the compact structure of the peptide ring backbones and the packed situation of the surfactin molecules contribute to the formation of intramolecular and intermolecular hydrogen bonds, the peptide ring that consists of seven amino acid residues is too short to form stable β -sheet conformation.

Figure 7 shows the radial distribution functions of the oxygen atoms in water molecules, O_w , with respect to the heavy atoms (the oxygen atoms and the nitrogen atoms) in surfactin head-groups, which are all normalized by the bulk density of water phase. The well-defined peaks of the radial distribution functions

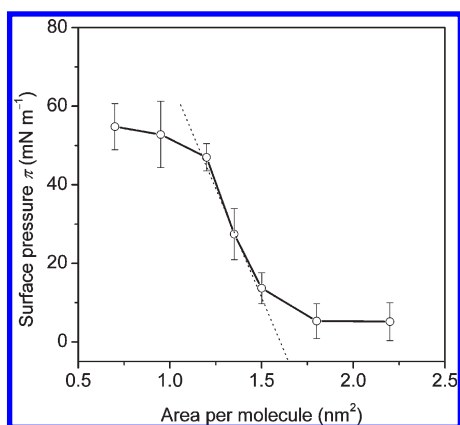


Figure 9. Surface pressure–area isotherm calculated from the simulation of the protonated surfactin monolayer at 293 K.

suggest that there is a significant hydration layer around the surfactin headgroups, and the width of the hydration layer of surfactin monolayer at the air/water interface is ~ 0.36 nm. The number of water molecules in the hydration layer per heavy atom decreases from 1.14 to 0.62 with the decrease of the molecular area from 2.20 to 0.70 nm^2 , indicating a dehydration process of the surfactin monolayer. Table 3 also shows the occupancy of hydrogen bonds formed between surfactin molecule and water, HB_{SW} . The key factors resulted in the reduction of HB_{SW} at higher interfacial concentration are the dehydration of the surfactin headgroups and the consequent lack of water molecules in the hydration layer, as well as the increase of HB_{SI} and HB_{SO} .

With the goal of better understanding the spatial arrangement of surfactin molecules at the air/water interface, Figure 8 displays the surfaces of both the hydrophobic and hydrophilic sides of the surfactin monolayer corresponding to the interfacial concentrations of 1.50 and $0.95 \text{ nm}^2 \text{ molecule}^{-1}$. As shown in Figure 8a, at a lower interfacial concentration the hydrophilic segments (blue and red) are dispersed at the monolayer surface of the hydrophilic side. When the surfactin molecules are in a more packed situation that shown in Figure 8b, the distribution of the hydrophilic segments is more concentrated and larger hydrophobic domains (green) are consequently presented at the surface of the hydrophilic side. The concentrative distribution of the hydrophilic segments may contribute to the formation of intermolecular hydrogen bonds, and the presence of the larger hydrophobic domains results in the dehydration of the monolayer. It can be easily observed from Figure 8 that the width of the monolayer increases with the interfacial concentration, and this argument is consistent with the analysis of the monolayer profiles and the molecular orientation.

3.4. Surface Pressure–Area Isotherm. Because the surface pressure (π) – area (A) isotherm is a crucial measure in experimental studies of surfactant monolayer, the surface pressure of the surfactin monolayer in our simulations is calculated as follows: $\pi = \gamma_0 - \gamma$, where γ_0 is the surface tension of pure water with a value of 72.75 mN m^{-1} at 293 K,³⁰ and γ is the surface tension of the air/water interface covered by a surfactin monolayer, which can be computed from the simulated trajectories using the following definition:³¹

$$\gamma = \frac{1}{2} \int_0^{L_z} \left(P_{zz} - \frac{P_{xx} + P_{yy}}{2} \right) dz \quad (1)$$

where P_{xx} , P_{yy} , and P_{zz} are the diagonal components of the averaged pressure tensor and L_z is the length of the simulating box along the

axis perpendicular to the air/water interface. Figure 9 shows the surface pressure–area isotherm of protonated surfactin monolayer at the air/water interface, and the isotherm is in a sigmoid shape. At a molecular area higher than 1.50 nm^2 , the surface pressure increases slowly. Surface pressure increases sharply and steadily with a further reduction of the molecular area to a value of 1.20 nm^2 , and the monolayer in this part of the isotherm is considered as an expanded monolayer. A plateau part observed at the molecular area lower than 0.95 nm^2 indicates that the monolayer is in a transition state. The intersection of the tangent to the isotherm of the expanded monolayer with the area axis (the dashed line in Figure 9) corresponds to the limiting molecular area, A_0 , and in this simulation the limiting molecular area is about 1.65 nm^2 for protonated *iso*-C15 surfactin molecules at 293 K. In addition, the compressibility coefficient of the expanded monolayer is $\sim 5.87 \text{ m N}^{-1}$ according to the relation, $\beta = -1/A_0(\partial A/\partial \pi)_T$.^{11,32} The surface pressures are seemed to be overestimated throughout, and this phenomenon is also showed in previous computer simulation of the surface pressure.³³

4. DISCUSSION

The orientation of surfactin molecules at the air/water interface is a favorable argument and several representative orientations have been proposed in previous studies. According to the compression isotherm curves of the protonated surfactin monolayer, Maget-Dana and Ptak¹¹ proposed that the peptide ring laid at the interface in an expanded monolayer, and the peptide ring gradually adopted a vertical orientation when the isotherm crossing a horizontal plateau. At the end of the horizontal plateau the peptide ring was perpendicular to the interface with a molecular area of $0.27 \pm 0.2 \text{ nm}^2$, and the surfactin molecules were over compressed in a solid monolayer. In the study of Ishigami et al.,⁴ the molecular orientation with the whole surfactin molecule lying on the interface was assumed to correspond to the A_0 value of $1.82\text{--}2.02 \text{ nm}^2$, and surfactin dimerization was formed by the hydrophobic interactions between the two alkyl chains. The A_t value of $0.79\text{--}0.89 \text{ nm}^2$ indicated that the alkyl chains vertically oriented to the interface plane and the peptide ring horizontally oriented on the interface. Our present simulation demonstrated that most of the peptide rings kept their supine orientation and slightly tilted at the air/water interface in an expanded monolayer, and the result was in agreement with the assumption of Maget-Dana and Ptak.¹¹ Similar conformation was suggested in the neutron reflectometry measurements of Shen et al.¹⁵ that the peptide rings aligned parallel with the surface even at a higher surface pressure. The difference is that the neutron reflectometry experiment was carried out at pH 7.5 and the surfactin molecule was expected to contain two carboxylate groups. Moreover, the vertical orientation of the peptide rings at the air/water interface was rarely detected even in an over compressed monolayer at an interfacial concentration of $0.70 \text{ nm}^2 \text{ molecule}^{-1}$ in the present simulation, this phenomenon not matched the hypothesis of the surfactin orientation at a horizontal plateau, but gave an indication of the structural flexibility of the peptide rings.

Unlike the hypothesis of Maget-Dana¹¹ and Ishigami,⁴ the vertical orientation of the aliphatic tails at the air/water interface was rarely detected even at the highest interfacial concentration of $0.70 \text{ nm}^2 \text{ molecule}^{-1}$ in the present simulation. The peptide moiety of the surfactin molecule is complex in structure comparing with most conventional synthetic surfactants, and thus even in a compressed monolayer where the peptide rings were in a packed situation, the aliphatic chains could not contact enough

with each other to adopt a vertical orientation on the interface. Moreover, the peptide moiety is composed of abundant hydrophobic residues, and there are occurrence of the hydrophobic contact between the aliphatic chain and the hydrophobic residue, which had been previously proposed.^{12,15,16} The hydrophobic residues that the aliphatic tails were preferential to contact with, Leu3 and Val4, were well matched the results obtained at the oil/water interface,^{34,35} and it could be assigned to a feature that the aliphatic tail, the Leu3 and Val4 residues all located on the hydrophobic side of the peptide ring. The hydrophobic contact between the aliphatic chains occurred on the upside of the aggregate in the present simulation, and this location was more logical than the assumption of Ishigami et al.⁴ that the alkyl chains laid on the air/water interface and contacted with each other by hydrophobic interactions.

The assumptions of the molecular orientation of surfactin in previous studies all ignored the structural flexibility of the peptide ring.^{4,11} The interfacial area was compared with the cross-sectional area of the peptide ring to judge whether the peptide ring tilted and how much of the gradient the peptide ring exhibited. The present study showed that the peptide rings at the air/water interface exhibited a structural variation as a function of the interfacial concentration. The peptide ring backbones adopted a more packed "horse-saddle" structure at higher interfacial concentration comparing with the expanded structure at lower interfacial concentration, and this was the evidence that the peptide ring backbone persisted for their horizontal orientation in a packed situation. Similar structural flexibility of protonated surfactin molecules were demonstrated by the molecular simulation at the oil/water interface.¹³ Surfactin headgroups were abundant in Leucine residues and these hydrophobic side chains largely contributed to the interfacial area of surfactin molecules.^{34,36} Our simulation illustrated that the orientation of the hydrophobic side chains should be considered in predicting the spatial arrangement of surfactin molecules at the air/water interface.

The β -turn structure of surfactin molecules at the air/water interface estimated by the intramolecular hydrogen bonds in this study is consistent with experimental studies of surfactin in DMSO.^{17,37} The β -sheet structure was detected in surfactin micelles by circular dichroism spectra in alkaline solutions.^{4,38} Though the β -sheet domains was observed in the protonated surfactin monolayer at the present simulation, the number of the hydrogen bonds in the β -sheet domains was limited and the conformation was not stable. One factor that resulted in the unstable β -sheet conformation is the limited length of the peptide backbone, and another probable reason is that the interfacial concentration is not high enough in the simulation.

The shape of the surface pressure–area isotherm evaluated in the present simulation is similar with the isotherms derived from experimental studies.^{4,11,12,14,18,38–40} The feature of the isotherm of the protonated surfactin monolayer distinguishing from that of charged surfactin monolayer, the solid state,^{11,18} was not shown here mainly due to the fact that the molecular area was not set lower than 0.70 nm^2 . The limiting molecular area A_0 estimated from the calculated isotherm, about 1.65 nm^2 , is well agreement with the values of $\sim 1.58 \text{ nm}^2$ and $\sim 1.70 \text{ nm}^2$ derived from the experimental surface pressure–area curves for protonated surfactin at 20°C .^{12,18} Recent neutron reflection study provided a little smaller area per surfactin molecule of 1.40 nm^2 at pH 6.5.¹⁶ The compressibility of the expanded monolayer based on this A_0 value is of the same magnitude order of $8.3 \pm 0.7 \text{ m N}^{-1}$ obtained at pH 3.03.¹¹ As had been described, the quite

horizontal plateau at a pressure was defined as the transition phase, in which region the surfactin molecules began to reorientate. The simulated transition phase began at a molecular area within a range of $0.95\text{--}1.20 \text{ nm}^2$ according to the simulated surface pressure–area isotherm, and the reorientation of the surfactin molecules in the transition phase reflected an apparent increment of the monolayer width as concluded above.

5. CONCLUSIONS

In this paper, we studied the properties of protonated surfactin monolayer adsorbed at the air/water interface by molecular dynamics simulation.

The results showed that both of the headgroups and the hydrophobic tails adopted a tilted orientation in an over compressed monolayer, otherwise most of peptide rings slightly tilted at the air/water interface in a supine position and the tails intended to approach the interface plane. The hydrophobic tails were favorable to fold back to interact with the Leu3 and Val4 residues, and the occurrence of the hydrophobic contact between surfactin molecules increased with the interfacial concentration, especially the interactions between the hydrophobic tails. The peptide ring backbones exhibited a structural flexibility that a more packed structure was adopted at a higher interfacial concentration. The root-mean-square deviations of the peptide ring backbones and the Ramachandran angles showed a smaller fluctuation in structure when the surfactin molecules in a more packed situation. The packed structure of the peptide rings benefited the formation of the intramolecular and intermolecular hydrogen bonds, and thus the hydrophobic contacts between surfactin molecules, the stability of the β -turn structure in Leu2 \rightarrow Asp5 and the β -sheet domains were consequently enhanced. The surface pressure–area isotherm of the protonated surfactin monolayer was simulated at 293 K. The limiting molecular area and the compressibility coefficient of the expanded monolayer were in well agreement with that obtained by experimental technique.

The simulations present detail information of the surface parameter of protonated surfactin molecules and the structural properties of the protonated surfactin monolayer adsorbed at the air/water interface. Further investigation should be focus on the properties of surfactin monolayer at different surrounding conditions at an atomistic level by molecular dynamics simulation, such as the influence of pH and the addition of electrolytes in the subphase.

■ ASSOCIATED CONTENT

S Supporting Information. Averaged matrix of the smallest distance between the residues within a surfactin molecule or belong to different surfactin molecules at different interfacial concentrations. This material is available free of charge via the Internet at <http://pubs.acs.org>.

■ AUTHOR INFORMATION

Corresponding Author

*Tel: +86-21-64252063; Fax: +86-21-64252485; E-mail: bzmu@ecust.edu.cn

■ ACKNOWLEDGMENT

This work has been supported by the China Postdoctoral Science Foundation (Grant No. 20100480610), the Shanghai Postdoctoral Sustentation Fund (Grant No. 11R21412400), and

the National High Technology Research and Development Program of China (Grant No. 2009AA063503).

REFERENCES

- (1) Liu, X. Y.; Yang, S. Z.; Mu, B. Z. *J. Pept. Sci.* **2008**, *14*, 864.
- (2) Li, Y. M.; Haddad, N. I.; Yang, S. Z.; Mu, B. Z. *Int. J. Pept. Res. Ther.* **2008**, *14*, 229.
- (3) Hue, N.; Serani, L.; Laprevote, O. *Rapid Commun. Mass Spectrom.* **2001**, *15*, 203.
- (4) Ishigami, Y.; Osman, M.; Nakahara, H.; Sano, Y.; Ishiguro, R.; Matsumoto, M. *Colloids Surf. B* **1995**, *4*, 341.
- (5) Peypoux, F.; Bonmatin, J. M.; Wallach, J. *Appl. Microbiol. Biot.* **1999**, *51*, 553.
- (6) Vollenbroich, D.; Ozel, M.; Vater, J.; Kamp, R. M.; Pauli, G. *Biologicals* **1997**, *25*, 289.
- (7) Tendulkar, S. R.; Saikumari, Y. K.; Patel, V.; Raghotama, S.; Munshi, T. K.; Balaram, P.; Chattoo, B. B. *J. Appl. Microbiol.* **2007**, *103*, 2331.
- (8) Kracht, M.; Rokos, H.; Ozel, M.; Kowall, M.; Pauli, G.; Vater, J. *J. Antibiot.* **1999**, *52*, 613.
- (9) Khire, J. M. *Adv. Exp. Med. Biol.* **2010**, *672*, 146.
- (10) Whang, L. M.; Liu, P. W.; Ma, C. C.; Cheng, S. S. *J. Hazard. Mater.* **2008**, *151*, 155.
- (11) Maget-Dana, R.; Ptak, M. *J. Colloid Interface Sci.* **1992**, *153*, 285.
- (12) Gallet, X.; Deleu, M.; Razafindralambo, H.; Jacques, P.; Thonart, P.; Paquot, M.; Brasseur, R. *Langmuir* **1999**, *15*, 2409.
- (13) Nicolas, J. P. *Biophys. J.* **2003**, *85*, 1377.
- (14) Song, C. S.; Ye, R. Q.; Mu, B. Z. *Colloid. Surf. A* **2007**, *302*, 82.
- (15) Shen, H. H.; Thomas, R. K.; Chen, C. Y.; Darton, R. C.; Baker, S. C.; Penfold, J. *Langmuir* **2009**, *25*, 4211.
- (16) Shen, H. H.; Lin, T. W.; Thomas, R. K.; Taylor, D. J. F.; Penfold, J. *J. Phys. Chem. B* **2011**, *115*, 4427.
- (17) Bonmatin, J. M.; Genest, M.; Labbe, H.; Ptak, M. *Biopolymers* **1994**, *34*, 975.
- (18) Deleu, M.; Paquot, M.; Jacques, P.; Thonart, P.; Adriaensen, Y.; Dufrene, Y. F. *Biophys. J.* **1999**, *77*, 2304.
- (19) Humphrey, W.; Dalke, A.; Schulten, K. *J. Mol. Graphics* **1996**, *14*, 33.
- (20) Berendsen, H. J. C.; Postma, J. P. M.; van Gunsteren, W. F.; Hermans, J. In *Intermolecular Forces*; Pullman, B., Ed.; D. Reidel: Dordrecht, The Netherlands, 1981; p 331.
- (21) Berendsen, H. J. C.; van der Spoel, D.; van Drunen, R. *Comput. Phys. Commun.* **1995**, *91*, 43.
- (22) Lindahl, E.; Hess, B.; van der Spoel, D. *J. Mol. Model.* **2001**, *7*, 306.
- (23) Jorgensen, W. L.; Maxwell, D. S.; Tirado-Rives, J. *J. Am. Chem. Soc.* **1996**, *118*, 11225.
- (24) Berendsen, H. J. C.; Postma, J. P. M.; DiNola, A.; Haak, J. R. *J. Chem. Phys.* **1984**, *81*, 3684.
- (25) Essmann, U.; Perera, L.; Berkowitz, M. L.; Darden, T.; Lee, H.; Pedersen, L. G. *J. Chem. Phys.* **1995**, *103*, 8577.
- (26) Ryckaert, J. P.; Ciccotti, G.; Berendsen, H. J. C. *J. Comput. Phys.* **1977**, *23*, 327.
- (27) Schweighofer, K. J.; Essmann, U.; Berkowitz, M. *J. Phys. Chem. B* **1997**, *101*, 3793.
- (28) Nicolas, J. P.; de Souza, N. R. *J. Chem. Phys.* **2004**, *120*, 2464.
- (29) van der Spoel, D.; Vogel, H. J.; Berendsen, H. J. C. *Proteins* **1996**, *24*, 450.
- (30) Lide, D., Ed.; *CRC Handbook of Chemistry and Physics*; CRC Press: Boca Raton, FL, 2002–2003.
- (31) Kaznessis, Y. N.; Kim, S.; Larson, R. G. *Biophys. J.* **2002**, *82*, 1731.
- (32) Duncan, S. L.; Larson, R. G. *Biophys. J.* **2008**, *94*, 2965.
- (33) Giner-Casares, J. J.; Camacho, L.; Martin-Romero, M. T.; Lopez Cascales, J. J. *Langmuir* **2008**, *24*, 1823.
- (34) Gang, H. Z.; Liu, J. F.; Mu, B. Z. *J. Phys. Chem. B* **2010**, *114*, 2728.
- (35) Gang, H. Z.; Liu, J. F.; Mu, B. Z. *J. Phys. Chem. B* **2010**, *114*, 14947.
- (36) Bonmatin, J. M.; Genest, M.; Petit, M. C.; Gincel, E.; Simorre, J. P.; Cornet, B.; Gallet, X.; Caille, A.; Labbe, H.; Vovelle, F.; Ptak, M. *Biochimie* **1992**, *74*, 825.
- (37) Ferre, G.; Besson, F.; Buchet, R. *Spectrochim. Acta A* **1997**, *53*, 623.
- (38) Zou, A. H.; Liu, J.; Garamus, V. M.; Yang, Y.; Willumeit, R.; Mu, B. Z. *J. Phys. Chem. B* **2010**, *114*, 2712.
- (39) Eeman, M.; Berquand, A.; Dufrene, Y. F.; Paquot, M.; Dufour, S.; Deleu, M. *Langmuir* **2006**, *22*, 11337.
- (40) Bouffieux, O.; Berquand, A.; Eeman, M.; Paquot, M.; Dufrene, Y. F.; Brasseur, R.; Deleu, M. *Biochim. Biophys. Acta* **2007**, *1768*, 1758.